JCTC Journal of Chemical Theory and Computation

Article

pubs.acs.org/JCTC

A Tuned LRC-DFT Design of Ambipolar Diketopyrrolopyrrole-Containing Quinoidal Molecules Interesting for Molecular Electronics

Gregorio García,[†,‡] José M. Granadino-Roldán,[‡] Alfonso Hernández-Laguna,[§] Andrés Garzón,[∥] and Manuel Fernández-Gómez*[,‡]

[†]Laboratoire d'Electrochimie, Chimie des Interfaces et Modélisation pour l'Energie, CNRS UMR-7575, Ecole Nationale Supérieure de Chimie de Paris, Chimie ParisTech, 11 rue Pierre et Marie Curie, 75231 Paris Cedex 05, France

[‡]Department of Physical and Analytical Chemistry, University of Jaén, Campus "Las Lagunillas" s/n, 23071, Jaén, Spain

[§]Instituto Andaluz de Ciencias de la Tierra, CSIC - University of Granada, Avda. de Las Palmeras no. 4, 18100, Armilla (Granada), Spain

[∥]Faculty of Pharmacy, University of Castilla-La Mancha, Paseo de los Estudiantes, s/n, 02071, Albacete, Spain

Supporting Information

ABSTRACT: This work presents a Density Functional Theory (DFT) study on the charge transport related properties of two quinoidal diketopyrrolopyrrole (DPP) based systems. System **A**, recently synthesized, shows high efficiency as *n*-type organic semiconductor material while system **B**, not synthesized yet, has a linking benzothiadiazole (BT) unit between DPP moieties and would display an ambipolar character. The use of tuned, long-range corrected (LRC) functionals allows one to predict HOMO, LUMO, and charge transport properties for compound **A** in concordance with those experimentally observed. The use of BT building blocks allows for a conclusion that compound **B** is expected to display balanced and efficient charge injection along with high mobilities both for holes and electrons, which points to its potential to obtain high performances as an ambipolar semiconductor.

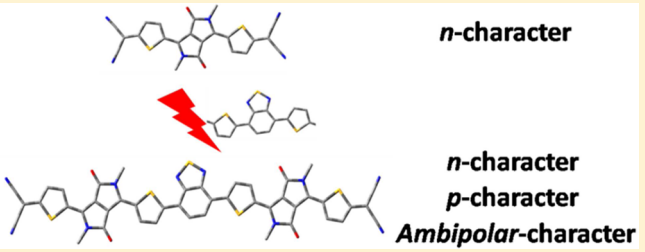

1. INTRODUCTION

Nowadays, there exists considerable interest in the use of electronic devices based on π-conjugated organic materials, such as organic field effect transistors (OFETs).[1,2] OFETs have garnered much attention due to their potential applications in a variety of optoelectronic devices, such as organic active-matrix displays, electronic identification, or electronic papers.[3,4] The design of low-power consumption complementary circuits needs the combination of *p*- and *n*-type materials.[5,6] However, the development of efficient *n*-type materials is lagging behind that of *p* materials, due to problems such as high electron injection barriers and low ambient stability of anionic species.[1,3,6] Interest has recently turned into the development of ambipolar materials, with both high and balanced electron and hole mobilities, due to their interest in a range of applications such as complementary-like logic circuits[7−10] and light-emitting field-effect transistors.[11−13]

Conjugated polymers based on diketopyrrolopyrrole (DPP) units are attracting great interest for their promising features in OFETs[14−19] and organic solar cells (OSCs)[16,17,20,21] due to their planarity, ability to form hydrogen bonds, and electron-poor nature. DPP is a desirable molecular building block because of its chemical stability and ease of synthesis and modification, and thus different substitutions have allowed for obtaining ambipolar copolymers. Hence, Chen et al. reported hole/electron mobilities as high as 0.35/0.40 $cm^2\ V^{-1}\ s^{-1}$ combining a donor−acceptor−donor moiety (thiophene−benzothiadiazole−thiophene) with DPP in diketopyrrolopyrrolethieno[3,2-b]thiophene copolymer,[14] while Sonar et al. reported also ambipolar character after substituting thiophene with furan in that copolymer.[18] Other examples include polymers made up of DPP−thienothiophene−thiophene−thiophene[14] and thienothiophene−DPP−benzodithiophene units.[16]

Materials based on small molecules can be a suitable alternative to conjugated polymers. Well-defined structures, ease of synthesis and functionalization, and no batch to batch variations are some of their advantages over conjugated polymers. It has recently been demonstrated that DPP-based molecules with quinoidal structure are also promising candidates for *n*-type semiconductors. In this sense, Qiao et al. have reported the synthesis, characterization, and application of a novel DPP-containing quinoidal small molecule to be used in OFETs (compound **A**, see Scheme 1).[22] It also needs to be stressed that ambipolar materials with high and balanced hole and electron mobilities are currently actively sought due to their great range of applicability in molecular electronics. In this

Received: January 31, 2013

   dx.doi.org/10.1021/ct4000845 | J. Chem. Theory Comput. XXXX, XXX, XXX−XXX

Scheme 1. Molecular Structure of Compound A along with Its Bond Labeling[a]

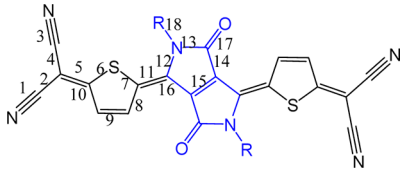

[a]The DPP unit is indicated in blue. R = 2-ethyl-hexyl.

regard, Zhang et al. have synthesized a DPP-based molecule linked to benzothiadiazole (BT), which showed an efficient ambipolar behavior.[23]

On the basis of these results, we have hypothesized that the modification of compound **A** with BT (compound **B**, see Scheme 2) should improve its ambipolar character. We must

Scheme 2. Molecular Structure of Compound B along with Its Bond Labeling[a]

i)

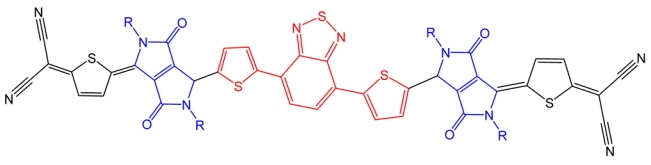

ii)

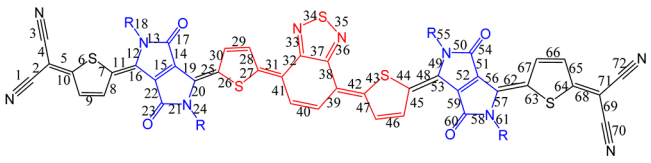

[a]The DPP and BT units are indicated in blue and red, respectively: (*i*) BT with aromatic character and (*ii*) BT with quinoid character. R = 2-ethyl-hexyl.

emphasize first that compound **B** has not yet been synthesized and, second, that to the best of our knowledge ambipolar transport has not been reported for DPP-based small molecules with quinoidal structure. Therefore, we were motivated to explore how the BT unit influences DPP-based molecules. In order to rationalize such effects, a detailed quantum chemical investigation of charge transport related properties is needed. Besides, a thorough theoretical study of compounds **A** and **B** focusing on the evaluation of the main parameters involved in charge transport will allow for obtaining information about the origin of *n*, *p*, and ambipolar semiconductor character. Thus, in this work we have studied from a density functional theory (DFT) perspective the effects of the BT unit on the crystal structure and charge transport related properties of DPP-based small molecules with quinoidal structure.

Main parameters related with the theoretical study of organic semiconductors are directly related with ionization potentials (IPs) and electron affinities (EAs). Unfortunately, it is well-known that, due to the self-interaction error (SIE), standard exchange-correlation functionals yield highest occupied/lowest unoccupied molecular orbital (HOMO/LUMO) energies which differ from the corresponding IPs/EAs. The so-called range-separated hybrid density functionals tend to minimize that SIE through the splitting of the Coulomb repulsion energy (see below) into a long-range term and a short-range one.[24−26]

When long-range is treated through full nonlocal Hartree−Fock exchange, this class of range-separated functional is called a long-range corrected (LRC) functional, thus improving the prediction of IPs, EAs, and related properties.[25]

In a range-separated functional, the range-separation parameter, ω, controls the length scale for the transition from the short-range to the long-range. This parameter is typically determined (semi-) empirically by fitting to a particular training set. However, results derived from LRC-DFT could be improved if the range-separation parameter is optimally tuned for each system under study by demanding that the DFT version of Koopmans' theorem be obeyed (see section 2.2).[25−27]

Thus, the main goal of this work is the theoretical study through a tuned LRC-DFT functional of the charge transport related properties for the above-mentioned compounds **A** and **B**. Besides, tuning the range-separation parameter (ω) will allow us to evaluate this methodology to improve the description of charge transport related properties through comparison with available experimental data for compound **A**.[22]

2. COMPUTATIONAL DETAILS

2.1. Crystal Structures. The corresponding crystal structures were optimized with a density functional theory (DFT) method by using the Dmol3 program code included in the Materials Studio package (MS).[28] Compound **A** crystal structure optimization was performed using a double-numerical + d, DND, basis set with a global orbital cutoff of 4.5 Å and 3 × 2 × 1 *k* points, within the Generalized-Gradient Approximation (GGA), using the Perdew−Burke−Ernzerhof (PBE) functional[29] included in MS. The larger number of atoms of compound **B** along with the available computational resources forced the electronic structure to be optimized with the same basis set and a global orbital cutoff of 3.6 Å, and only in Γ point. Optimizations were performed at the cell parameters and atomic positions. For compound **A** (**B**) the defined energy and gradient optimization convergence thresholds were 1×10^{-5} (2×10^{-5}) Ha and 2×10^{-2} (4×10^{-3}) Ha/Å, respectively, while the displacement and maximum displacement convergence thresholds were 5×10^{-2} (5×10^{-3}) and 0.3 (0.3) Å, respectively.

2.2. Range-Separation Parameter Tuning. Salzner and Aydin compared the ability of a number of functionals to predict properties of π-conjugated oligomers, concluding that the ωB97 family produces generally smaller errors than any of the other range-separated functionals.[30] We have then selected the long-range corrected hybrid density functional ωB97X (with ω = 0.3 bohr^{-1}) since it has been proven to perform better than other well-established functionals and has been recommended for general use in chemistry.[31] Range-separated functionals split the Coulomb operator into long-range (LR) and short-range (SR) through the standard error function (erf) and the complementary standard error function (erfc), respectively:[25,26]

$$\frac{1}{r} = \frac{\mathrm{erf}(\omega r)}{r} + \frac{\mathrm{erfc}(\omega r)}{r} \quad (1)$$

where the range separation is determined by a single parameter ω. Then, $1/2\omega$ corresponds to the distance at which the Coulomb operator changes from being mostly described by the

dx.doi.org/10.1021/ct4000845 | J. Chem. Theory Comput. XXXX, XXX, XXX−XXX

Table 1. Unit Cell Parameters for Compounds A and B (In Parentheses Relative Errors) and Root Mean Square Deviations (RMSD) between the Experimental and Optimized Structure (PBE) of A for Bond Lengths and Atomic Positions

	unit cell parameters					
	a/Å	b/Å	c/Å	α/deg	β/deg	γ/deg
A	8.69 (3.82%)	10.46 (4.4%)	14.47 (2.7%)	97.9 (0.5%)	104.8 (0.0%)	110.3 (0.3%)
B	9.93	19.84	18.37	106.86	90.67	101.97
experimental[a]	8.37	10.02	14.09	98.4	104.8	110.0
					RMSD/Å	
	bond lengths				0.020	
	atomic positions				0.301	

[a]For compound **A**, taken from ref 22.

SR term (erfc) to be described mostly by the LR (erf) one. Thus, the main effect of the ω parameter is to control the length scale for range separation in the studied system.[32] However, the ω parameter is typically determined by fitting its value to a particular training set. An alternative is the optimization of the range-separation parameter for each system of interest.[25]

A frequently used approach is to optimize ω by enforcing that the DFT analog to Koopmans' theorem is obeyed; i.e., the HOMO eigenvalue ($\varepsilon_{\mathrm{HOMO}}$) of the neutral system (N electrons) has approximately to equal to minus the ionization potential (IP):[33] $\varepsilon_{\mathrm{HOMO}} = -\mathrm{IP}$. Thus, the IP-optimized ω, from now on ω_{HOMO}, is obtained so that[25,26]

$$-\varepsilon^{\omega}_{\mathrm{HOMO}(N)} = \mathrm{IP}^{\omega}(N) \equiv E_{\mathrm{gs}}(N-1;\omega) - E_{\mathrm{gs}}(N;\omega) \tag{2a}$$

$$\Delta\mathrm{IP} = \varepsilon^{\omega}_{\mathrm{HOMO}(N)} + \mathrm{IP}^{\omega}(N) = 0 \tag{2b}$$

where the ionization potential is calculated as the energy difference between the total, ground state energies (E_{gs}) of the relaxed, N, and $N-1$ electron systems with the same value of ω. This approach has been proven to allow a quantitative prediction of ionization potentials[26] and HOMO energies[25] without empirical considerations. However, an equivalent approach to obtain electron affinities and LUMO energies is not possible since an analogous "Koopman's theorem" that relates the LUMO energy to the electron affinity (EA) does not exist. Nevertheless, this problem can be circumvented considering that the IP of the $N+1$ electron anion is the same as the EA of the N electron system, i.e., to seek a ω such that[26]

$$-\varepsilon^{\omega}_{\mathrm{HOMO}(N+1)} = \mathrm{IP}^{\omega}(N+1) \equiv E_{\mathrm{gs}}(N;\omega) - E_{\mathrm{gs}}(N+1;\omega) \tag{3}$$

Equations 2 and 3 provide two different conditions, wherein only ω has to be optimized. Thus, we can decrease the overall error minimizing the target function, $J(\omega)$:[26]

$$J^2(\omega) = (\varepsilon_{\mathrm{HOMO(N)}} + \mathrm{IP}(N))^2 + (\varepsilon_{\mathrm{HOMO}(N+1)} + \mathrm{IP}(N+1))^2 \tag{4}$$

Finally, replacing $\varepsilon_{\mathrm{HOMO}(N+1)}$ with $\varepsilon_{\mathrm{LUMO}(N)}$ should yield an alternative optimization criterion for ω, from now on ω_J:[26]

$$J^2(\omega_J) = (\varepsilon^{\omega}_{\mathrm{HOMO}(N)} + \mathrm{IP}(N))^2 + (\varepsilon_{\mathrm{LUMO}(N)} + \mathrm{IP}(N+1))^2 \tag{5}$$

This way, we have optimized ω_{HOMO} (from eq 2) and ω_J (from eq 5) for compounds **A** and **B**. The range-separation parameter optimization was carried out at the ωB97X/6-31G** level. Basis sets containing diffuse functions are recommended to get a higher accuracy in the calculation of energy-related properties such as electronic excitation energies, ionization potentials, or electron affinities.[34] Hence, ω was also optimized for compound **A** at the ωB97X/6-31+G** level, using the geometries optimized at the same level of theory. SCF convergence problems prevented us from using diffuse functions with compound **B**, although after a comparison of the results obtained with and without diffuse functions for compound **A** we can conclude that the approximation works well. That result could be expected bearing in mind that the optimization of the ω parameter pursues the improvement on the accuracy of HOMO and LUMO related properties, and therefore, similar results for HOMO and LUMO related properties should be obtained regardless of the basis set employed.

2.3. Molecular Geometries and Charge Transport Related Properties. Ground neutral and charged state geometries of both systems were optimized by using the ωB97X functional along with the 6-31G** basis set. As some experimental data for compound **A** were obtained in solution, ground state geometries were also optimized at the same level taking into account solvent effects (CH_2Cl_2) by means of a continuum solvation movel (IEFPCM).[35,36] Then, using ωB97X/6-31G** optimized geometries, properties such as excitation energies (by means of TD-DFT formalism), HOMO and LUMO energies, ionization potentials, electron affinities, intramolecular reorganization energies, and charge transfer integrals were calculated using the default value for ω (ω_{d} from now on), ω_{HOMO}, and ω_J for each compound. Excitation energies and HOMO/LUMO energies were also calculated taking into account solvent effects. In the case of **A**, these properties were also obtained with ω parameters obtained for the 6-31+G** basis set.

The charge transfer integral for a cluster of two molecules extracted from the previously optimized crystal structure was obtained following the so-called projective method,[37,38] according to which the Fock's matrix is written in terms of localized orbitals by using the orbital projection; i.e., we project the molecular orbitals (MOs) of the selected dimer of stacked molecules on a basis set defined by the MOs of the individual molecules. Thus, from the energy values of the MOs of the dimer, we can get the Fock matrix elements on the basis of the MOs of the single molecules. This procedure was carried out with the *J-from-g03* code.[37,38]

dx.doi.org/10.1021/ct4000845 | J. Chem. Theory Comput. XXXX, XXX, XXX−XXX

All the calculations described in the two last sections were performed with Gaussian 09 (revision B.01).[39] In order to reduce the computational cost, these calculations were carried out with R = methyl (see Schemes 1 and 2), since Qiao et al. have established that variation of the alkyl groups on the nitrogen atom in the DPP moiety has almost no effect on the electronic structure of compound **A**.[22] Also, it has been proven that the increase of the side chain length does not influence charge transport related properties such as HOMO and LUMO energies, EA, IP and λ_i (see e.g. refs 40 and 41).

3. RESULTS

3.1. Crystal Structures. To the best of our knowledge, there are reported crystal parameters only for compound **A**.[22] Table 1 shows experimental and optimized unit cell parameters, and Table 1S gathers Cartesian coordinates along with translation vectors for both theoretical unit cells obtained by using the PBE functional. In the case of compound **A**, the departure of the calculated unit cell parameters from the experimental values lies in the range 0.0−4.4%. Table 1 also collects root-mean-square deviations (RMSD) between experimental and optimized bond lengths and atomic positions for compound **A**, whose values are 0.020 Å and 0.309 Å, respectively. As can be seen, PBE can be considered a rather accurate method for optimizing both the unit cell parameters containing two molecules of solvent, $CHCl_3$, and the molecular atomic geometry of **A**. Also, for designing compound **B** it was necessary to add two molecules of solvent, $CHCl_3$, per unit cell in order to optimize the crystal structure.

Both compounds show crystal structures with only one molecule per unit cell. In Figures 1 and 2, a representation of both crystal structures along the *a* axis and a couple of π-stacked molecules can be seen. In both cases, the π-conjugated backbone assumes a near planar conformation (which is also noted in the experimental crystal structure of **A**). Conjugated backbones lead to a columnar π-stacking structure, wherein molecules adopt a slipped face to face arrangement along the molecular axis (see Figure 2), whose π-stacking distances are 3.57 and 3.38 Å for compounds **A** (experimental value is 3.395 Å) and **B**, respectively. Besides, while the stacked backbones of **A** show waved paralleled planar displaced molecules, **B** shows straight, more-overlapping stacked structures, which should allow one to think of a stronger interaction between molecules.

It is well-known, however, that local, gradient corrected functionals, like PBE, show shortcomings at the adequate description of long-range (dispersion) interaction forces that are commonly believed the most important in organic molecular crystals. Bearing in mind the experimental structure of crystal **A** is reasonably well reproduced by our PBE calculations (see Table 1), we may think that van der Waals interactions are not the only driving force for the bonding mechanism in this type of compounds.[42,43] Since **A** and **B** are narrowly related compounds, we may also expect that PBE behaves reasonably well for the latter.

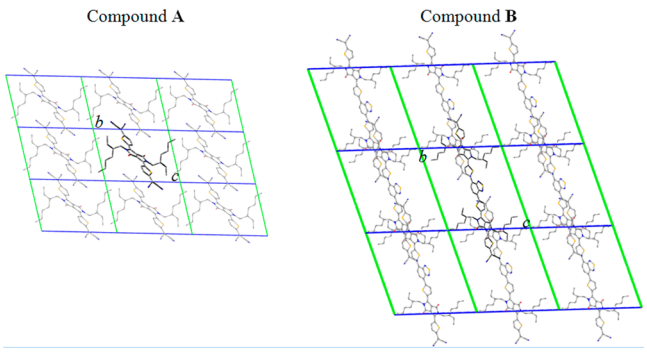

Figure 1. Theoretical crystal structures along the *ab* plane (solvent molecules and H atoms are omitted for clarity).

3.2. Molecular Geometries. Impact of Charge Injection on Molecular Geometry. Tables 2S and 3S collect ωB97X/6-31G** gas-phase optimized bond lengths for neutral, cationic, and anionic species of compounds **A** and **B** (similar results were obtained for **A** at the ωB97X/6-31+G** level). As it is well-known, compound **A** shows a quinoidal structure.[22] For this compound, our calculations yield CC distances for bonds 5, 9, 11, and 15 (see Scheme 1 for bond labeling) lying in the range 1.346−1.365 Å, which are near to a typical C=C double bond distance (1.33 Å). Bonds 8, 10, and 16 show bond lengths around 1.456 Å, shorter than a typical C−C single bond (1.54 Å) and longer than a typical C=C bond, which points to single bonds with some double bond character. This quinoidal structure should mainly be due to the electron-withdrawing effect of CN groups. For **B**, calculated distances for bonds 5, 9, 11, 15, 52, 62, 66 and 68/8, 10, 16, 56, 67, and 64 (see Scheme 2 for bond labeling) are indicative that these could be also considered as double C=C bonds/single C−C bonds with some double bond character. The BT moiety in compound **B** has lost its aromatic character (see Scheme 2, *i*), acquiring a quinoidal structure (see Scheme 2, *ii*). For example, bonds 29, 31, and 40 can be considered formal C=C double bonds, while distances of bonds 28 and 32 are closer to a typical C−C single bond distance. Therefore, **B** would also show a quinoidal structure.

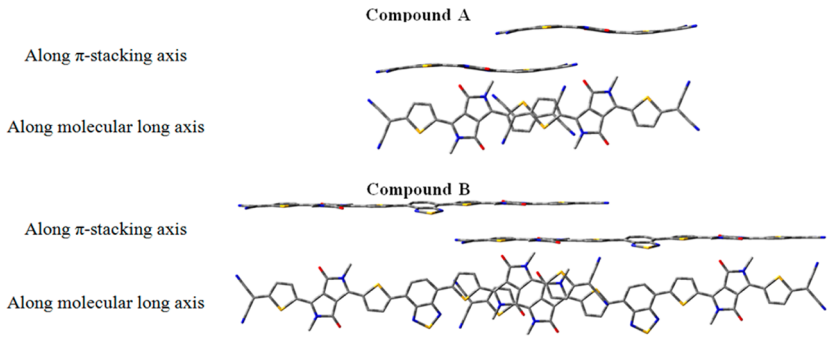

Figure 2. Schematic representation of a dimer for compounds **A** and **B**. Hydrogen atoms and alkyl side chains have been omitted.

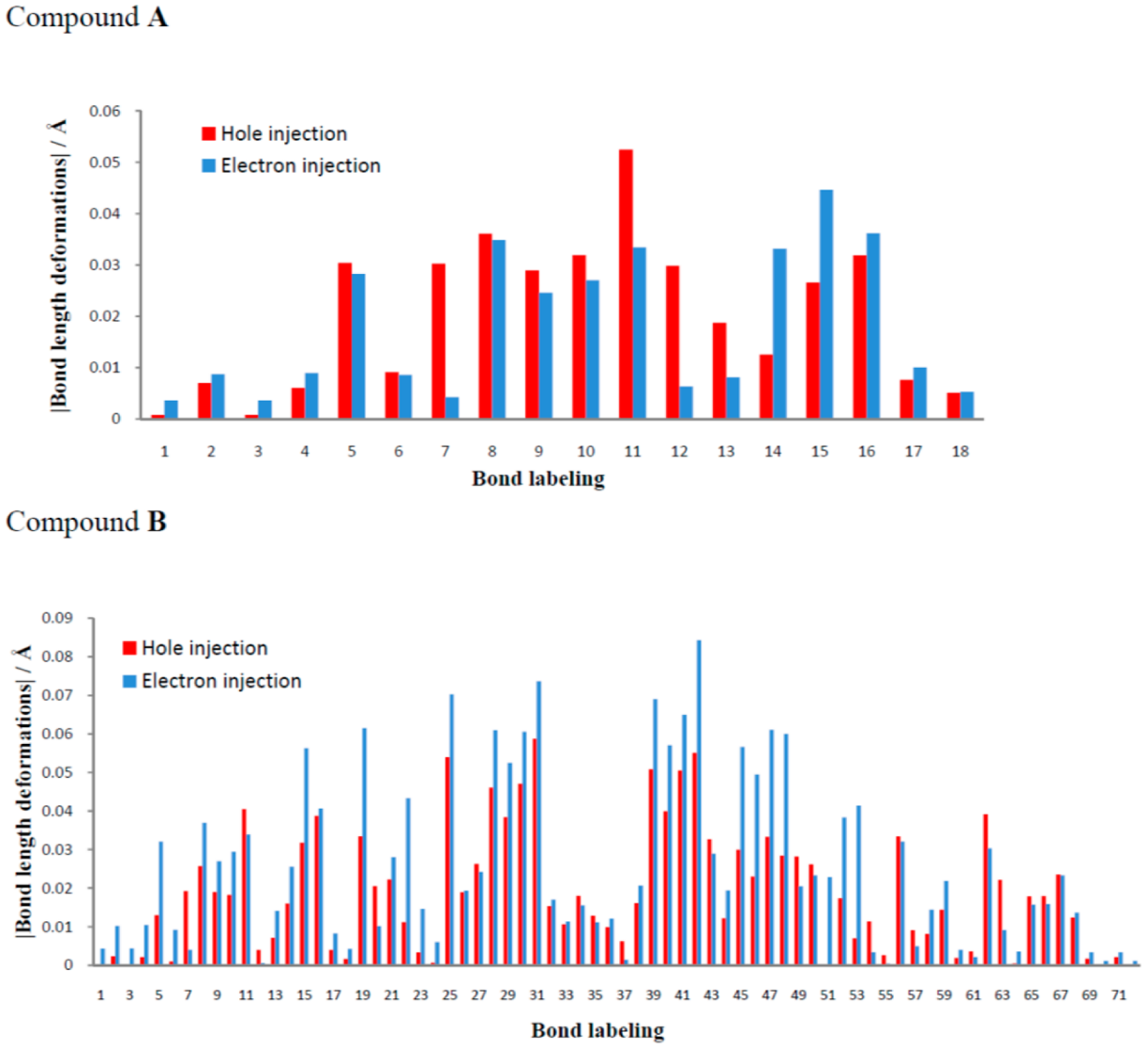

Figure 3. Bond length deformations (Å) between neutral and charged states of each system.

The impact of charge injection on molecular structure can be visualized in Figures 3 and 4, from which it is inferred that single C−C bonds become shorter, while C═C double bonds become longer. This is indicative that some quinoid character is lost as a result of charge injection. It is also shown in Figures 3 and 4 that the geometry of compound **A**/**B** is more influenced by hole/electron injection, although most of the bonds show to be sensitive both to hole and electron injection. As can be seen, the injected charge (both holes and electrons) is allocated near DPP and BT units, while injected electrons are also accommodated on the terminal thiophene rings.

The changes on molecular geometry due to hole/electron injection can be related to the shape of HOMO/LUMO orbitals (see Figure 5). For example, the HOMO of compound

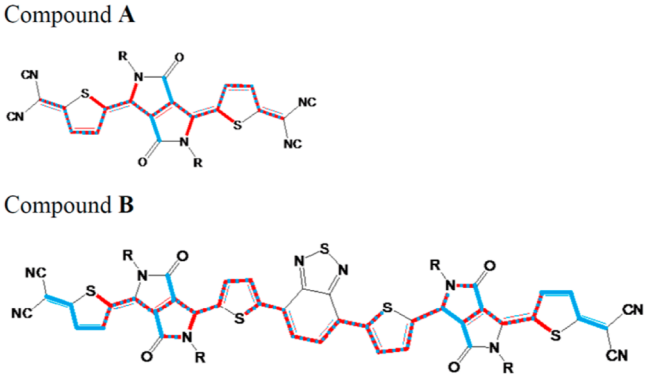

Figure 4. The most affected bonds (length change ≥ 0.02 Å) for hole (red) or electron (blue) injection.

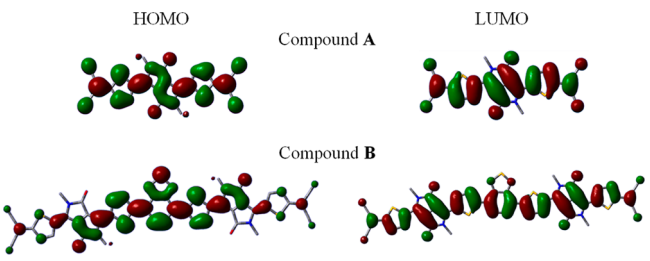

Figure 5. Electronic density contours of HOMO and LUMO orbitals of compounds **A** and **B**.

dx.doi.org/10.1021/ct4000845 | J. Chem. Theory Comput. XXXX, XXX, XXX−XXX

B spreads mainly over DPP and BT units, which are the motifs most influenced by hole injection. However, the LUMO is delocalized over the whole molecule, which is in concordance with the fact that nearly all bonds show a greater sensitivity to electron injection.

3.3. Range-Separation Parameter Tuning. Table 2 collects the value of the different range-separation parameters obtained for compounds **A** and **B** according to eqs 2 and 5, while Figure 1S plots the evolution of |ΔIP| (which is minimized to calculate ω_{HOMO}) and J^2 (which is also minimized to calculate ω_J) as a function of the ω parameter. Table 3 shows charge transport related properties obtained using ω_d, ω_{HOMO}, and ω_J, along with the experimental values for compound **A**. As concerns the effect of the basis set, it can be seen how in the case of **A** the values of ω_{HOMO} and ω_J decrease by just 0.004 bohr^{-1} when a diffuse function is added. As already pointed out by Körzdörfer et al.[25] and Stein et al.,[44] the ω parameter is expected to decrease with the size of the conjugated π system. This trend is observed for compound **B**, for which both optimized ω_{HOMO} and ω_J are lower than their counterparts for compound **A**. The large size of the systems under study can also be related to the rather high deviation of the range-separation parameter from its default value. In all cases (see Table 2), ω_J is smaller than ω_{HOMO}. As can be seen in Table 3, the influence of the basis set size on the predicted properties is, in general, bigger when ω_d is used, whereas when using ω_{HOMO} and ω_J a much less sensitivity is displayed (the biggest difference turns out to be 0.22 eV for the adiabatic electron affinity, AEA, of compound **A**), despite the 6-31G** basis set requiring much less computational effort.

Table 2. Optimized ω Parameters for Compounds A and B Using the 6-31G Basis Set[a]**

	ω_d	ω_{HOMO}	ω_J
A	0.3	0.099 (0.095)	0.088 (0.084)
B	0.3	0.035	0.021

[a]In parentheses values for compound **A** using the 6-31+G** basis set. Units are in bohr^{-1}.

As expected, the accuracy with which HOMO and LUMO energies (E_{HOMO}, E_{LUMO}) and optical bandgap (E_{opt}) are predicted improves when any optimized range-separation parameter other than the default one is used. Thus, the differences between experimental and theoretical values for E_{opt} decrease from 0.78 eV at the ωB97X/6-31G** level with ω_d to 0.34 and 0.32 eV with ω_{HOMO} and ω_J, respectively. The differences also decrease when the solvent is implicitly taken into account. Similar tendencies are obtained for E_{HOMO} and E_{LUMO}. As concerns LUMO energies, there are higher differences between experimental and theoretical values, and their values are more influenced by the use of ω_{HOMO} or ω_J, obtaining the best values, as expected, using ω_J. It is important to point out that the use of ω_J allows for obtaining better results not only for E_{LUMO} but also for the other experimental values.

Besides, ω_{HOMO} and ω_J were optimized according to eqs 2 and 5, respectively. Thus, the use of ω_J not only allows minimizing $|E_{HOMO}| - IP|$ but also $|E_{LUMO}| - EA|$ and consequently renders a proper value of the fundamental gap. Hence, we conclude that the use of ω_J is a good choice when corrections for HOMO and LUMO levels are needed.

In the case of **B**, ω parameters are lower than those for compound **A**, and thus they depart largely from the default value. As a result, the differences between values calculated with ω_d and those from tuned ω are even larger. The differences between results from ω_{HOMO} and ω_J are approximately the same as for compound **A**, with the exception of vertical and adiabatic ionization potentials.

3.4. Charge Transport Related Properties. It is well established that the efficiency of an organic semiconductor mainly depends on both the ease of injecting electrons/holes on its LUMO/HOMO orbitals and the mobility of charge carriers.

3.4.1. Reorganization Energies, Charge Transfer Integrals, and Charge Transfer Rates. In organic semiconductor materials, the charge hopping process is the predominant one at temperatures of practical technological applications, so that it has herein been selected to model the mobilities of charge carriers within our systems.[45] The charge hopping process is generally described as a self-exchange charge-transfer reaction between two neighboring molecules. When these two molecules are equivalent, the charge transfer rate, which is directly related with the hopping mobility (μ), can be defined according to the semiclassical Marcus theory as[45]

$$k_{ET} = \frac{4\pi^2}{h}\frac{1}{\sqrt{4\pi\lambda k_B T}}t^2 \exp\left[\frac{-\lambda}{4k_B T}\right] \quad (6)$$

where λ (reorganization energy) and t (charge transfer integral) are the two key parameters. It must be stressed out that the simplicity of this model renders values for transfer rates that must only be considered as ideal, superior limits. Thus, Marcus theory should be used as a first approximation.[46,47]

The reorganization energy is determined by fast changes in molecular geometry (the inner contribution) and by slow variations in polarization of surrounding medium (the outer contribution): $\lambda = \lambda_i + \lambda_o$. In the case of an ordered, organic crystal, only the inner contribution to λ should be taken into account (the outer contribution is on the order of a tenth of an electronvolt) as opposite to charge transfer in solution wherein the external part dominates.[45,48] Intramolecular reorganization energies (λ_i) were calculated as indicated in ref 45. Taking into account the definition of IP and EA, λ_i can be expressed as a function of IP and EA, and thus λ_i was calculated using the different essayed range-separation parameters (see Supporting Information for information on the expressions used to calculate λ_i).

Intramolecular reorganization energies are collected in Table 3. For compound **A**, regardless of the value of the ω parameter, similar reorganization energies are obtained for both 6-31G** and 6-31+G** basis sets. As concerns the effect of the ω value for both compounds **A** and **B**, ω_d always yields the largest values, while those using ω_{HOMO} and ω_J (for holes as well as for electrons) are similar. This result agrees with that obtained by Körzdöfer et al.[49] according to which the default range-separation parameter renders a significant overlocalization of the excess charge for linear, conjugated systems. As a result, using the default range-separation parameter will lead to an overestimation of the reorganization energy for this kind of system. The tuning of the range-separation parameter diminishes the delocalization error, and thus, reorganization energy and charge transfer constants obtained this way should be more reliable than those obtained from other functionals.

Comparison between both compounds allows one to conclude that λ_i^+ and λ_i^- are similar for compound **B** while the differences are bigger in the case of compound **A** (being

dx.doi.org/10.1021/ct4000845 | J. Chem. Theory Comput. XXXX, XXX, XXX−XXX

Table 3. Charge Transport Related Properties for Compounds A and B, along with Experimental Values

		ω_d		ω_{HOMO}		ω_J	
	exptl.[a]	6-31+G**	6-31G**	6-31+G**	6-31G**	6-31+G**	6-31G**
				compound **A**			
E_{opt} (gas)/ eV		2.30	2.24	2.18	2.21	2.15	2.19
E_{opt} (dis. CH_2Cl_2)/eV	1.73	2.47	2.51	2.04	2.07	2.01	2.05
E_{HOMO} (gas)/eV		−8.58	−8.34	−7.24	−7.10	−7.13	−7.00
E_{HOMO} (dis. CH_2Cl_2)/eV	−6.24	−8.23	−8.02	−6.91	−6.79	−6.91	−6.70
AIP/eV		7.70	7.48	7.24	7.10	7.21	7.08
VIP/eV		7.99	7.78	7.47	7.34	7.44	7.31
$\|E_{HOMO}$ (gas)$\|$ − AIP$\|$/eV		0.88	0.86	0.00	0.00	0.08	0.07
E_{LUMO} (gas)/eV		−3.04	−2.78	−3.46	−3.27	−3.52	−3.33
E_{LUMO} (dis. CH_2Cl_2)/eV	−4.51	−2.64	−1.07	−3.11	−2.93	−3.16	−2.98
AEA/eV		3.90	3.61	3.63	3.41	3.60	3.40
VEA/eV		3.60	3.30	3.22	3.01	3.18	2.99
$\|E_{LUMO}$ (gas)$\|$ − AEA$\|$/eV		0.86	0.83	0.17	0.15	0.08	0.07
λ_i^+/eV		0.60	0.60	0.42	0.41	0.41	0.41
$\|t_{HOMO}\|$/eV			0.09		0.08		0.08
$K_{ET}^+ \times 10^{-12}/s^{-1}$			0.51		3.10		3.10
λ_i^-/eV		0.64	0.66	0.33	0.34	0.31	0.32
$\|t_{LUMO}\|$/eV			0.12		0.11		0.11
$K_{ET}^- \times 10^{-12}/s^{-1}$			0.48		12.73		15.95
K_{ET}^+/K_{ET}^-			1.06		0.24		0.19
				compound **B**			
E_{opt} (gas)/ eV			1.85		1.36		1.34
E_{opt} (dis. CH_2Cl_2)/eV			1.66		1.17		1.16
E_{HOMO} (gas)/eV			−7.07		−5.46		−5.30
E_{HOMO} (dis. CH_2Cl_2)/eV			−6.77		−5.18		−5.03
AIP/eV			5.84		5.45		5.88
VIP/eV			6.09		5.62		6.03
$\|E_{HOMO}$(gas)$\|$ − AIP$\|$/eV			1.22		0.00		0.14
E_{LUMO} (gas)/eV			−2.64		−3.51		−3.63
E_{LUMO} (dis. CH_2Cl_2)/eV			−2.40		−3.28		−3.41
AEA/eV			4.02		3.79		3.79
VEA/eV			3.77		3.64		3.64
$\|E_{LUMO}$(gas)$\|$ − AEA$\|$/eV			1.38		0.29		0.15
λ_i^+/eV			0.52		0.32		0.31
$\|t_{HOMO}\|$/eV			0.12		0.13		0.12
$K_{ET}^+ \times 10^{-12}/s^{-1}$			2.12		22.27		21.25
λ_i^-/eV			0.49		0.30		0.30
$\|t_{LUMO}\|$/eV			0.13		0.13		0.12
$K_{ET}^- \times 10^{-12}/s^{-1}$			3.44		27.95		23.81
K_{ET}^+/K_{ET}^-			0.62		0.80		0.89
K_{ET}^A/K_{ET}^B							
holes			0.24		0.14		0.15
electrons			0.14		0.46		0.67

[a]Experimental value measured in CH_2Cl_2, taken from ref 22.

always $\lambda_i^+ > \lambda_i^-$). Reorganization energies are always lower in the case of compound **B** irrespective of both the nature of the charge carrier and ω. According to eq 6, low λ_i values are first needed to obtain high transfer rates even though the charge transfer integral, t, also plays a very important role.

The charge transfer integral (see Table 3) describes the probability of electron tunneling between two neighboring molecules, so it depends on their relative arrangement.[45] Charge transfer integrals were calculated from a cluster of two molecules (extracted from the crystal structure) using the projective method. Both compounds **A** and **B** show a single charge pathway along π-stacking arrangements (see Figure 2). As charge transfer integrals strongly depend on the overlap between molecular orbitals, there are only slight differences between the values obtained using different range-separation parameters. The largest values of charge transfer integrals were obtained for compound **B**, whose values for holes and electrons are around 0.13 eV while for compound **A**, $|t_{LUMO}|$ (~0.11 eV) turns out to be somewhat higher than $|t_{HOMO}|$ (~0.08 eV).

Taking into account the relative disposition between molecules within the crystal (Figure 2) and the shape of HOMO and LUMO orbitals (Figure 5), we note that in the case of **A** there is an overlap between molecular orbital (MO) fragments over quinoidal thiophene rings and the CN group. This overlap seems to be more favorable to obtaining a larger $|t_{LUMO}|$. Compound **B** shows a greater overlap, which could be due to the nonwaved and more-overlapping stacked structure of **B**, which should yield larger interaction between molecules.

dx.doi.org/10.1021/ct4000845 | J. Chem. Theory Comput. XXXX, XXX, XXX−XXX

Concretely, there is an overlap between MO fragments belonging to different molecules, one of them located on the DPP unit and the other on the quinoidal thiophene one. This larger overlap between frontier orbitals in **B** leads to higher charge transfer integrals for both holes and electrons.

Once the intramolecular reorganization energies and charge transfer integrals are calculated, the charge transfer rates (Table 3) can be estimated according to eq 6. Hole and electron mobilities for compound **B** were predicted to be higher than those for compound **A**. The K_{ET}^{+}/K_{ET}^{-} ratio, also shown in Table 3, allows for seeing how the pronounced *n*-character reported for compound **A**[22] is only predicted with tuned range-separation parameters. In the case of compound **B**, the K_{ET}^{+}/K_{ET}^{-} ratio is in all cases lower than and closer to unity (~0.80), which is indicative of a balanced hole/electron mobility. Besides, as said before, both electron and hole mobilities are higher than their compound **A** counterparts. It is important to emphasize that both high and balanced mobilities are requested to obtain ambipolar materials.

3.4.2. Charge Injection. The efficiency of charge injection is mainly determined by the injection barrier height at the metal-semiconductor interface, which is controlled by the energy difference between the work function of the injecting metal, Φ_m, and the (gas) ionization level (HOMO) and the (gas) affinity level (LUMO) of the semiconductor for hole and electron injection, respectively, corrected for interface dipoles.[50,51] These interface dipoles come from either partial charge transfer, with or without interface chemistry, between the metal and the semiconductor, the reduction of the metal work function by the organic layer (except when a large charge transfer to the metal surface takes place), and occupation of the metal-induced density of interface states (IDIS) in the gap of the organic material.[52,53] As a result, the gap between semiconductor affinity and ionization levels at the metal/organic interface narrows up to several electronvolts as compared to the gas-phase, frontier energy levels (see, e.g., refs 51, 54, and 55).

Experimental information about changes in the metal Φ_m can be obtained from UPS and Kelvin probe methods, while IP and EA can be obtained from PES and IPES, respectively, although EA is usually estimated from IP and the HOMO−LUMO gap deduced from the optical band gap.[51,55,56]

Any model intended for a complete description of the metal/organic interface, far beyond the aim of this paper, should account for the various specific interactions appearing at the metal/semiconductor interface. This is why the knowledge of the free metal work function and that of the (gas) HOMO/LUMO levels cannot give much information but a guidance about the levels' alignment at the interface and, therefore, to the electron/hole barrier injection as well as about trends within a set of related compounds.[52] Thus, one can obtain qualitative information about charge injection efficiency through the $\Phi_m - |E_{HOMO/LUMO}|$ difference.[3,4,52,57]

For an efficient hole/electron injection, besides adequate HOMO/LUMO levels, low/high IPs/EAs are also desirable.[5] Ionization potentials and electron affinities are also related to air instability and charge transfer efficiency.[5]

Figure 6 plots HOMO and LUMO energies for compounds **A** and **B** predicted using ω_{HOMO} and ω_J (see Table 3), along with the (free) electrode work function energies of most common metals used for hole and electron injection. In the case of **A**, the cyclic voltammetry HOMO/LUMO energy values when dissolved in CH_2Cl_2 are −6.24 eV/−4.51 eV.[22]

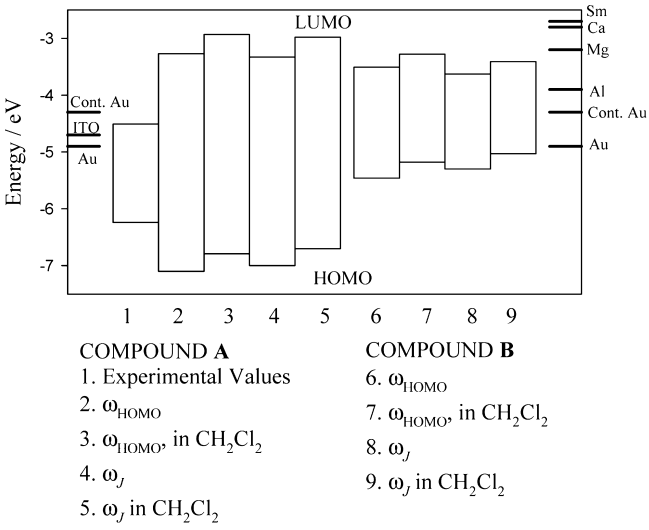

Figure 6. HOMO and LUMO energy levels along with free metal work functions. Experimental values were taken from ref 22.

The low value of the work function for Au (Φ_m = −4.9 eV) suggests an efficient electron injection. However, the HOMO energy is far from the electrode work function of free typical metals used as anodes, such as indium tin oxide, ITO (Φ_m = −4.7 eV), and Au (Φ_m = −4.9 eV).[58] Thus, disregarding the above-mentioned surface and interface dipoles, not considered here, devices based on compound **A** are expected to exhibit *n*-type semiconducting character.[22] This feature is correctly predicted, since although the LUMO energy is estimated to be worse than the HOMO one, HOMO/LUMO energies calculated, e.g., using ω_J, are far from/close to the work function of metals used as anodes/cathodes. Hence, electron injection would still be more efficient, which along with the already analyzed larger electron mobilities for compound **A** would explain its pronounced *n*-character.[22]

Following the same train of thought, compound **B** has a predicted LUMO energy level slightly deeper than that for compound **A**, which means that this compound could show a similar efficiency for electron injection. Regarding the E_{HOMO} values calculated upon range-separation optimized parameters, they become close to the work functions of ITO and Au, which allows one to think of an easy hole injection. In ambipolar devices, the hole and electrons should be injected from the same electrode, usually the Au electrode, which seems to be feasible in the case of compound **B**. Besides, it is known that compounds with LUMO energies lower than −3.15 eV could show ambipolar character.[59] A balanced hole and electron injection barrier could also help to obtain an ambipolar behavior, which would be possible from a contaminated Au electrode (Φ = −4.3 eV).[60] Thus, we conclude that compound **B** is expected to show efficient hole and electron injection from the Au electrode, which along with the predicted high and balanced mobilities both for holes and electrons points to its suitability to obtain high efficiencies in ambipolar devices.

Another requisite to be fulfilled for a stable *n*-type material is to get an EA of, at least, 3.0 eV but not much greater than 4.0 eV, the upper limit for which a too electrophilic molecule could be unstable in ambient conditions.[61] Devices based on **A** show ambient stability, which agrees with the calculated EA values. As seen in Table 3, both compounds show predicted EAs using tuned ω parameters within this range. For an efficient hole

injection, low IPs are desirable. However, too low IPs would lead to unintentional doping, and therefore to low ON/OFF ratios.[62] Fortunately, calculated IPs, regardless of the tuned ω parameter used, are larger than those obtained for typical *p*-type materials, such as poly(3-hexylthiophene) (IP ∼ 5.0 eV), which shows unintentional doping.[62] Hence, compound **B** would be safe from suffering unintentional doping. All these factors would enhance the ambient stability and performance of devices based on compound **B**.

4. CONCLUSIONS

Compounds **A** (a recently synthesized quinoidal DPP-containing small molecule with high efficiency as an *n*-type organic semiconductor) and **B** (a modification of compound **A** with BT units) have been investigated by means of DFT to elucidate their suitability as precursors of organic semiconductors. Moreover, aimed at obtaining improved values of HOMO and LUMO related properties, the ω parameter of the long-range corrected hybrid functional ωB97X was tuned enforcing the fulfilment of the DFT analog to Koopman's theorem. The following conclusions can be derived from this work:

Regarding the use of tuned long-range corrected functionals: (i) Optimization of the ω parameter in the ωB97X functional has allowed obtainment of theoretical values which compare better with experimental values for optical bandgap, HOMO, and LUMO energies than ω_d in the case of compound **A**. Small differences are obtained between the theoretical values upon using ω_{HOMO} and ω_J, although the use of the ω_J allows one to obtain better results not only for E_{LUMO} but also for the other experimental values. (ii) In the case of compound **A**, we have also tested the effect of basis set (6-31G** and 6-31+G**). Although there are differences between the calculated ω parameters as a function of the basis set, similar and significant values of HOMO and LUMO related properties are obtained regardless of the basis set essayed.

Regarding the optimization of crystal structures: (iii) Both compounds show only one molecule per unit cell, which leads to columnar π-stacked structures, whose π-stacking distance is around 3.5 Å. In the case of compound **A**, there is a good agreement between experimental and theoretical crystal structures. In the case of **B**, there is a large overlapping between molecules, which leads to larger charge transfer integrals.

Regarding charge transport related properties: (iv) Compound **A**, as expected, shows higher electron than hole mobilities and a more efficient electron injection; both factors are in agreement with the high proved efficiency of **A** as an *n*-type organic semiconductor. (v) Compound **B** is expected to have higher charge (hole and electron) mobilities than **A**. Both hole and electron mobilities are balanced for compound **B**. As concerns charge injection, **B** would show similar electron injection efficiency to **A**, since **B** provides similar values for HOMO and LUMO energies. Hole injection from the Au electrode would also be efficient for compound **B**. Thus, compound **B** is predicted to show both efficient hole and electron injections and also high and balanced hole and electron mobilities, factors related to high efficiencies in ambipolar materials.

In summary, the employed theoretical methodology has shown to be able to reproduce the pronounced *n*-character of **A**. Besides, we have been able to conclude that the modification of a quinoidal DPP based-system with BT units would lead to quinoidal compounds with improved charge transport related properties, which in turn would be adequate as precursors of ambipolar materials.

■ ASSOCIATED CONTENT

Ⓢ Supporting Information

Expressions used for ionization potentials, electron affinities, intramolecular reorganization energies, Cartesian coordinates along with translation vectors (Tv) for both optimized unit cells, bond lengths for compounds **A** and **B** at the ωB97X/6-31G** level, evolution of $|\Delta IP|$ and J^2 as a function of the ω parameter, and predicted adiabatic ionization potentials and electron affinities. This information is available free of charge via de Internet at http://pubs.acs.org.

■ AUTHOR INFORMATION

Corresponding Author

*E-mail: mfg@ujaen.es.

Notes

The authors declare no competing financial interest.

■ ACKNOWLEDGMENTS

Support from Consejería de Innovación, Ciencia y Empresa, Junta de Andalucía (Spain) (PAI-FQM-337 contract) is gratefully acknowledged. We also thank Dr. J. Kirkpatrick (Oxford University) for allowing us the use of the *J-from-g03* code.

■ REFERENCES

(1) Malachowski, M. J.; Zmija, J. Organic field-effect transistors. *Opto-Electron. Rev.* **2010**, *18*, 121−136.

(2) Ruiz, C.; García-Frutos, E. M.; Hennrich, G.; Gómez-Lor, B. Organic Semiconductors toward Electronic Devices: High Mobility and Easy Processability. *J. Phys. Chem. Lett.* **2012**, *3*, 1428−1436.

(3) Wen, Y.; Liu, Y. Recent progress in n-channel organic thin-film transistors. *Adv. Mater.* **2010**, *22*, 1331−1345.

(4) Yan, L.; Zhao, Y.; Wang, X.; Wang, X. Z.; Wong, W. Y.; Liu, Y.; Wu, W.; Xiao, Q.; Wang, G.; Zhou, X.; Zeng, W.; Li, C.; Wang, X.; Wu, H. Platinum-based poly(aryleneethynylene) polymers containing thiazolothiazole group with high hole mobilities for field-effect transistor applications. *Macromol. Rapid Commun.* **2012**, *33*, 603−609.

(5) Newman, C. R.; Frisbie, C. D.; Filho, D. A. S.; Brédas, J. L.; Ewbank, P. C.; Mann, K. R. Introduction to Organic Thin Film Transistors and Design of n-Channel Organic Semiconductors. *Chem. Mater.* **2004**, *16*, 4436−4451.

(6) Usta, H.; Facchetti, A.; Marks, T. J. n-Chanel Semiconductor Materials Design for Organic Complementary Circuits. *Acc. Chem. Res.* **2011**, *44*, 501−510.

(7) Anthopoulos, T. D.; de Leeuw, D. M.; Cantatore, E.; Setayesh, S.; Meijer, E. J.; Tanase, C.; Hummelen, J. C.; Blom, P. W. M. Organic complementary-like inverters employing methanofullerene-based ambipolar field-effect transistors. *Appl. Phys. Lett.* **2004**, *85*, 4205−4207.

(8) Chen, Z.; Lemke, H.; Albert-Seifried, S.; Caironi, M.; Nielsen, M. M.; Heeney, M.; Zhang, W.; McCulloch, I.; Sirringhaus, H. High Mobility Ambipolar Charge Transport in Polyselenophene Conjugated Polymers. *Adv. Mater.* **2010**, *22*, 2371−2375.

(9) Bijleveld, J. C.; Zoombelt, A. P.; Mathijssen, S. G. J.; Wienk, M. M.; Turbiez, M.; de Leeuw, D. M.; Janssen, R. A. J. Poly-(diketopyrrolopyrrole-terthiophene) for ambipolar logic and photovoltaics. *J. Am. Chem. Soc.* **2009**, *131*, 16616−16617.

(10) Roelofs, W. S. C.; Mathijssen, S. G. J.; Bijleveld, J. C.; Raiteri, D.; Geuns, T. C. T.; Kemerink, M.; Cantatore, E.; Janssen, R. A. J.; de Leeuw, D. M. Fast ambipolar integrated circuits with poly-(diketopyrrolopyrrole- terthiophene). *Appl. Phys. Lett.* **2011**, *98*, 203301−203303.

(11) Zaumseil, J.; Friend, R. H.; Sirringhaus, H. Spatial control of the recombination zone in an ambipolar light-emitting organic transistor. *Nat. Mater.* **2006**, *5*, 69−74.
(12) Chen, Z.; Fang, J.; Gao, F.; Brenner, T. J. K.; Banger, K. K.; Wang, X.; Huck, W. T. S.; Sirringhaus, H. Enhanced charge transport by incorporating additional thiophene units in the poly(fluorene-thienyl-benzothiadiazole) polymer. *Org. Electron.* **2011**, *12*, 461−471.
(13) Gwinner, M. C.; Khodabakhsh, S.; Giessen, H.; Sirringhaus, H. Simultaneous Optimization of Light Gain and Charge Transport in Ambipolar Light-Emitting Polymer Field-Effect Transistors. *Chem. Mater.* **2009**, *21*, 4425−4433.
(14) Chen, Z.; Lee, M. J.; Ashraf, R. S.; Gu, Y.; Albert-Seifried, S.; Nielsen, M. M.; Schroeder, B.; Anthopoulos, T. D.; Heeney, M.; McCulloch, I.; Sirringhaus, H. High-Performance Ambipolar Diketopyrrolopyrrole-Thieno[3,2-*b*]thiophene Copolymer Field-Effect Transistors with Balanced Hole and Electron Mobilities. *Adv. Mater.* **2012**, *24*, 647−652.
(15) Kanimozhi, C.; Yaacobi-Gross, N.; Chou, K. W.; Amassian, A.; Anthoupoulos, T. D.; Patil, S. Diketopyrrolopyrrole-diketopyrrolopyrrole-based conjugated copolymer for high-mobility organic field-effect transistors. *J. Am. Chem. Soc.* **2012**, *134*, 16532−16535.
(16) Tandy, K.; Dutta, G. K.; Zhang, Y.; Venkatramaiah, N.; Aljada, M.; Burn, P. L.; Meredith, P.; Namdas, E. B.; Patil, S. A new diketopyrrolopyrrole-based co-polymer for ambipolar field-effect transistors and solar cells. *Org. Electron.* **2012**, *13*, 1981−1988.
(17) Li, Y.; Sonar, P.; Singh, S. P.; Ooi, Z. E.; Lek, E. S. H.; Loh, M. Q. Y. Poly(2,5-bis(2-octyldodecyl)-3,6-di(furan-2-yl)-2,5-dihydropyrrolo[3,4-*c*]pyrrole-1,4-dione-*co*-thieno[3,2-*b*]thiophene): a high performance polymer semiconductor for both organic thin film transistors and organic photovoltaics. *Phys. Chem. Chem. Phys.* **2012**, *14*, 7162−7169.
(18) Sonar, P.; Foong, T. R. B.; Singh, S. P.; Li, Y.; Dodabalapur, A. A furan-containing conjugated polymer for high mobility ambipolar organic thin film transistors. *Chem. Commun.* **2012**, *48*, 8383−8385.
(19) Jung, J.; Liu, F.; Russell, T. P.; Jo, W. H. A high mobility conjugated polymer based on dithienothiophene and diketopyrrolopyrrole for organic photovoltaics. *Energy Environ. Sci.* **2012**, *5*, 6857−6861.
(20) Li, W.; Roelofs, W.S. C.; Wienk, M. M.; Janssen, R. A. J. Enhancing the Photocurrent in Diketopyrrolopyrrole-Based Polymer Solar Cells via Energy Level Control. *J. Am. Chem. Soc.* **2012**, *134*, 13787−13795.
(21) Qu, S.; Tian, H. Diketopyrrolopyrrole (DPP)-based materials for organic photovoltaics. *Chem. Commun.* **2012**, *48*, 3039−3051 (and references therein).
(22) Qiao, Y.; Guo, Y.; Yu, C.; Zhang, F.; Xu, W.; Liu, Y.; Zhu, D. Diketopyrrolopyrrole-containing quinoidal small molecules for high-performance, air-stable, and solution-processable n-channel organic field-effect transistors. *J. Am. Chem. Soc.* **2012**, *134*, 4084−4087.
(23) Zhang, Y.; Kim, C.; Lin, J.; Nguyen, T. Q. Solution-Processed Ambipolar Field-Effect Transistor Based on Diketopyrrolopyrrole Functionalized with Benzothiadiazole. *Adv. Funct. Mater.* **2012**, *22*, 97−105.
(24) Savin, A.; Flad, H.-J. Density functionals for the Yukawa electron-electron interaction. *Int. J. Quantum Chem.* **1995**, *56*, 327−332.
(25) Körzdörfer, T.; Sears, J. S.; Sutton, C.; Brédas, J. L. Long-range corrected hybrid functionals for π-conjugated systems: Dependence of the range-separation parameter on conjugation length. *J. Chem. Phys.* **2011**, *135*, 204107−204112.
(26) Kronik, L.; Stein, T.; Refaely-Abramson, S.; Baer, R. Excitation Gaps of Finite-Sized Systems from Optimally Tuned Range-Separated Hybrid Functionals. *J. Chem. Theory Comput.* **2012**, *8*, 1515−1531.
(27) Stein, T.; Kronik, L.; Baer, R. Reliable Prediction of Charge Transfer Excitations in Molecular Complexes Using Time-Dependent Density Functional Theory. *J. Am. Chem. Soc.* **2009**, *131*, 2818−2820.
(28) Delley, B. An all-electron numerical method for solving the local density functional for polyatomic molecules. *J. Chem. Phys.* **1990**, *92*, 508−517.
(29) Perdew, J. P.; Burke, K.; Ernzerhoz, M. Generalized Gradient Approximation Made Simple. *Phys. Rev. Lett.* **1996**, *77*, 3865−3868.
(30) Salzner, U.; Aydin, A. Improved Prediction of Properties of π-Conjugated Oligomers with Range-Separated Hybrid Density Functionals. *J. Chem. Theory Comput.* **2011**, *7*, 2568−2583.
(31) Chai, J. D.; Head-Gordon, M. Systematic optimization of long-range corrected hybrid density functional. *J. Chem. Phys.* **2008**, *128*, 084106−084120.
(32) Jiménez-Hoyos, C. A.; Janesko, B. G.; Scuseria, G. E. Evaluation of range-separated hybrid density functionals for the prediction of vibrational frequencies, infrared intensities, and Raman activities. *Phys. Chem. Chem. Phys.* **2008**, *10*, 6621−6629.
(33) Cramer, C. J.; Trular, D. G. Density functional theory for transitions metals and transition metal chemistry. *Phys. Chem. Chem. Phys.* **2009**, *11*, 10757−10816.
(34) Foresman, J. B.; Frisch; A. E. *Exploring Chemistry with Electronic Structure Methods*, 2nd ed Gaussian, Inc.: Pittsburg, PA, 1996; p 149.
(35) Miertus, S.; Scrocco, E.; Tomasi, J. Electrostatic interaction of a solute with a continuum. A direct utilization of *ab initio* molecular potentials for the prevision of solvent effects. *Chem. Phys.* **1981**, *55*, 117−129.
(36) Barone, V.; Cossi, M. Quantum Calculation of Molecular Energies and Energy Gradients in Solution by a Conductor Solvent Model. *J. Phys. Chem A* **1998**, *102*, 1995−2001.
(37) Kirkpatrick, J. An approximate method for calculating transfer integrals based on the ZINDO Hamiltonian. *Int. J. Quantum Chem.* **2008**, *108*, 51−56.
(38) Baumeier, B.; Kirkpatrick, J.; Andrienko, D. Density-functional based determination of intermolecular charge transfer properties for large-scale morphologies. *Phys. Chem. Chem. Phys.* **2010**, *12*, 11103−11113.
(39) Frisch, M. J.; Trucks, G. W.; Schlegel, H. B.; Scuseria, G. E.; Robb, M. A.; Cheeseman, J. R.; Scalmani, G.; Barone, V.; Mennucci, B.; Petersson, G. A.; Nakatsuji, H.; Caricato, M.; Li, X.; Hratchian, H. P.; Izmaylov, A. F.; Bloino, J.; Zheng, G.; Sonnenberg, J. L.; Hada, M.; Ehara, M.; Toyota, K.; Fukuda, R.; Hasegawa, J.; Ishida, M.; Nakajima, T.; Honda, Y.; Kitao, O.; Nakai, H.; Vreven, T.; Montgomery, J. A., Jr.; Peralta, J. E.; Ogliaro, F.; Bearpark, M.; Heyd, J. J.; Brothers, E.; Kudin, K. N.; Staroverov, V. N.; Kobayashi, R.; Normand, J.; Raghavachari, K.; Rendell, A.; Burant, J. C.; Iyengar, S. S.; Tomasi, J.; Cossi, M.; Rega, N.; Millam, J. M.; Klene, M.; Knox, J. E.; Cross, J. B.; Bakken, V.; Adamo, C.; Jaramillo, J.; Gomperts, R.; Stratmann, R. E.; Yazyev, O.; Austin, A. J.; Cammi, R.; Pomelli, C.; Ochterski, J. W.; Martin, R. L.; Morokuma, K.; Zakrzewski, V. G.; Voth, G. A.; Salvador, P.; Dannenberg, J. J.; Dapprich, S.; Daniels, A. D.; Farkas, O.Foresman, J. B.; Ortiz, J. V.; Cioslowski, J.; Fox, D. J. *Gaussian 09*, revision B.01; Gaussian, Inc.: Wallingford, CT, 2010.
(40) García, G.; Garzón, A.; Granadino-Roldán, J. M.; Moral, M.; Fernández-Liencres, M. P.; Navarro, A.; Fernández-Gómez, M. The Role of Linear Alkyl and Alkoxy Side Chains in the Modulation of the Structure and Electrical Properties of Bithiophene: a Theoretical Study. *Aust. J. Chem.* **2010**, *63*, 1297−1306.
(41) Granadino-Roldán, J. M.; Garzón, A.; García, G.; Moral, M.; Navarro, A.; Fernández-Liencres, M. P.; Peña-Ruiz, T.; Fernández-Gómez, M. Theoretical Study of the Effect of Alkyl and Alkoxy Lateral Chains on the Structural and Electronic Properties of π-Conjugated Polymers Consisting of Phenylethynyl-1,3,4-thiadiazole. *J. Phys. Chem. C* **2011**, *115*, 2865−2873.
(42) Hummer, K.; Pusching, P.; Ambrosch-Draxl, C. Ab initio study of anthracene under high pressure. *Phys. Rev. B* **2003**, *67*, 184105/1−184105/7.
(43) Provencer, F.; Bérubé, N.; Lapdrade, J. F.; Simard, G.; Tant, J.; de Halleux, V.; Geerts, Y.; Silva, C.; Côté, M. Large electronic bandwidth in solution-processable pyrene crystals. The role of the close-packed crystal structure. *J. Chem. Phys.* **2012**, *137*, 034706/1−034707/9.
(44) Stein, T.; Eisengerg, H.; Kronick, L.; Baer, R. Fundamental Gaps in Finite Systems from Eigenvalues of a Generalized Kohn-Sham Method. *Phys. Rev. Lett.* **2010**, *105*, 266802/1−266802/4.

(45) Wang, L.; Nan, G.; Yang, X.; Peng, Q.; Li, Q.; Zhigang, S. Computational methods for design of organic materials with high charge mobility. *Chem. Soc. Rev.* **2010**, *39*, 423−434.
(46) Troisi, A. Charge transport in high mobility molecular semiconductors: classical models and new theories. *Chem. Soc. Rev.* **2011**, *40*, 2347−2358.
(47) Rühle, V.; Lukyanov, A.; May, F.; Schrader, M.; Vehoff, T.; Kirkpatrick, J.; Baumeier, D.; Andrienko, D. Microscopic Simulations of Charge Transport in Disordered Organic Semiconductors. *J. Chem. Theory Comput.* **2011**, *7*, 3335−3345.
(48) McMahon, P.; Troisi, A. Evaluation of the External Reorganization Energy of Polyacenes. *J. Phys. Chem. Lett.* **2010**, *1*, 941−946.
(49) Körzdörfer, T.; Parrish, R. M.; Sears, J. S.; Sherrill, C. D.; Brédas, J. L. On the relationship between bond-length alternation and many-electron self-interaction error. *J. Chem. Phys.* **2012**, *137*, 124305/1−124305/8.
(50) Cheng, X.; Noh, Y. Y.; Wang, J.; Tello, M.; Frisch, J.; Blum, R. P.; Vollmer, A.; Rabe, J. P.; Koch, N. T.; Sirringhaus, H. Controlling Electron and Hole and Charge Injection in Ambipolar Organic Field-Effect Transistors by Self-Assembled Monolayers. *Adv. Funct. Mater.* **2009**, *19*, 2407−2415.
(51) Amy, F.; Chan, C.; Kahn, A. Polarization at the gold/pentacene interface. *Org. Electron* **2005**, *6*, 85−91.
(52) Natali, D.; Caironi, M. Charge Injection in Solution-Processed Organic Field-Effect Transistors: Physics, Models and Characterization Methods. *Adv. Mater.* **2012**, *24*, 1357−1387.
(53) Crispin, X.; Geskin, V.; Crispin, A.; Cornil, J.; Lazzaroni, R.; Salaneck, W. R.; Brédas, J. L.. Characterization of the Interface Dipole at Organic/Metal Interfaces. *J. Am. Chem. Soc.* **2002**, *124*, 8131−8141.
(54) Neaton, J. B.; Hybertsen, M. S.; Louie, S. G. Renormalization of Molecular Electronic Levels at Metal-Molecule interfaces. *Phys. Rev. Lett.* **2006**, *97*, 216405/1−216405/5.
(55) Ishii, H.; Sugiyama, K.; Ito, E.; Seki, K. Energy Level Alignment and Interfacial Electronic Structures at Organic/Metal and Organic/Organic interfaces. *Adv. Mater.* **1999**, *11*, 605−625.
(56) Schroeder, P. G.; France, C. B.; Park, J. B.; Parkinson, B. A. Orbital Alignment and Morphology of Pentacene Deposited on Au(111) and SnS2 Studied Using Photoemission Spectroscopy. *J. Phys. Chem. B* **2003**, *107*, 2253−2261.
(57) Chen, X. K.; Zou, L. Y.; Huang, S.; Min, C. G.; Ren, A. M.; Feng, J. K. Theoretical investigation of charge injection and transport properties of novel organic semiconductor materials—cyclic oligothiophenes. *Org. Electron.* **2011**, *12*, 1198−1210.
(58) Sworakowski, J.; Ulanski, J. Electrical properties of organic materials. *Annu. Rep. Prog. Chem., Sect. C: Phys. Chem.* **2003**, *99*, 87−125.
(59) Yoon, M. H.; DiBenedetto, S. A.; Russell, M. T.; Facchetti, A.; Marks, T. J. High-Performance n-Channel Carbonyl-Functionalized Quaterthiophene Semiconductors: Thin-Film Transistor Response and Majority Carrier Type Inversion via Simple Chemical Protection/Deprotection. *Chem. Mater.* **2007**, *19*, 4864−4881.
(60) Grobosch, M.; Knupfer, M. Charge-Injection Barriers at Realistic Metal/Organic Interfaces: Metals Become Faceless. *Adv. Mater.* **2007**, *19*, 754−756.
(61) Jansson, E.; Jan, P. C.; Agren, H. Density functional study of triazole and thiadiazole systems as electron transporting materials. *Chem. Phys.* **2006**, *330*, 166−171.
(62) Reséndiz, L.; Estrada, M.; Cerdeira, A.; Iñiquez, B.; Deen, M. J. Effect of active layer thickness on the electrical characteristics of polymer thin film transistors. *Org. Electron.* **2010**, *11*, 1920−1927.